BIOPHYSICS

Plus and minus ends of microtubules respond asymmetrically to kinesin binding by a long-range directionally driven allosteric mechanism

Huong T. Vu[1], Zhechun Zhang[2], Riina Tehver[3], D. Thirumalai[4]*

Although it is known that majority of kinesin motors walk predominantly toward the plus end of microtubules (MTs) in a hand-over-hand manner, the structural origin of the stepping directionality is not understood. To resolve this issue, we modeled the structures of kinesin-1 (Kin1), MT, and the Kin1-MT complex using the elastic network model and calculated the residue-dependent responses to a local perturbation in the constructs. Kin1 binding elicits an asymmetric response that is pronounced in α/β-tubulin dimers in the plus end of the MT. Kin1 opens the clefts of multiple plus end α/β-tubulin dimers, creating binding-competent conformations, which is required for processivity. Reciprocally, MT induces correlations between switches I and II in the motor and enhances fluctuations in adenosine 5′-diphosphate and the residues in the binding pocket. Our findings explain both the directionality of stepping and MT effects on a key step in the catalytic cycle of kinesin.

INTRODUCTION

The motor protein, kinesin, uses chemical energy generated by adenosine 5′-triphosphate (ATP) hydrolysis to transport organelles and vesicles and drives the motility of spindles and chromosomes inside the cell. To carry out these functions, it interacts with microtubule (MT), an important component of the cytoskeleton. For example, conventional kinesin, referred to as Kin1, walks on MT, assembled from tubulin dimer, toward the plus end of MT (*1*–*5*), in the process transporting organelles from the nucleus toward the cell membrane. In contrast, kinesin-13, part of the kinetochore that tethers chromosome, depolymerizes the spindle MT to drive chromosome segregation during mitosis (*6*). In much of the discussions of the kinesin stepping mechanism, it is tacitly assumed that MT may be treated as a passive polar track (*7*). Not only does MT affect the stepping of the motors, but it also affects other functions involving transportation (*8*–*11*). In particular, the kinesin-MT interaction sets the stepping direction and enhances rate-limiting adenosine 5′-diphosphate (ADP) release by about three orders of magnitude (*12*). The goal of the present study is to provide a structural explanation for the origin of directionality in the Kin1 stepping using the notion of local stiffness changes in the tubulin dimers and the motor, triggered by Kin1-MT interactions.

We were motivated to undertake this study based on the following observations: (i) It is known that kinesin-MT interaction affects the MT (*13*). For instance, Kin1 alters the MT lattice upon binding (*14*, *15*), thus establishing that the MT is not merely a static stiff polar track but plays a dynamic role in controlling the motility of the motor. (ii) We have shown previously that, after the tethered head detaches and stochastically diffuses toward the next binding site on the MT (*7*, *16*), the Kin1-MT interaction poises the free head to bind with the correct orientation (*7*). (iii) Expansion of the MT lattice induced by Kin1 binding (*10*, *14*, *15*) and even removal of α/β dimers when the motor steps on MT (*17*) show that the polar track must play a dynamic role.

Here, we use the structural perturbation method (SPM) (*18*, *19*), within the framework of normal mode analysis of the kinesin-MT complex (*20*–*22*), to calculate the changes in the residue fluctuations in kinesin and MT. The SPM calculations are used to address the following questions: (i) Are there residue-dependent responses in kinesin upon MT binding and vice versa, and how can they be quantified? (ii) Is the response of αβ-tubulin at the plus and minus ends of the MT distinct? (iii) Why does motor binding at a specific site on the MT promote other kinesin molecules to bind to the same MT (*14*, *23*)? (iv) Does the kinesin-induced expansion of the MT lattice (*14*, *15*) promote binding of other kinesins preferentially toward the plus end of the MT?

We answer these questions by first piecing together different Protein Data Bank (PDB) structures for kinesin and MT to create kinesin-MT complexes. Next, we created elastic network models (ENMs) in which contacts present within a cutoff distance in the complexes are assumed to interact via harmonic potentials. The eigenvalues and eigenvectors of the ENM (see Materials and Methods) and how they change upon perturbation are used to assess the residue-dependent dynamic responses throughout the different complexes, thus allowing us to answer the questions posed above. Binding of Kin1 to the MT produces an asymmetric response with residues in the β-tubulin exhibiting larger fluctuations than in the α-tubulin. Unexpectedly, the asymmetric response, which is more prominent in the plus-end tubulin dimers, propagates spatially across the MT protofilament. Kin1 binding at the cleft of the intradimer interface of a specific α/β results in a transition from a closed cleft (CC) to an open cleft (OC) state. The mechanical stress created in this process poises the downstream (plus end) α/β dimers to be in the OC states, which enhances the probability of the motor stepping toward the plus end, thus minimizing backward steps. As a corollary, it follows that upon binding of a single Kin1, other motors would preferentially bind to the sites on the plus end of the MT.

[1]Centre for Mechanochemical Cell Biology, Warwick Medical School, Coventry CV4 7AL, UK. [2]Department of Molecular and Cellular Biology, Harvard University, Cambridge, MA 02138, USA. [3]Department of Physics, Denison University, Granville, OH 43023, USA. [4]Department of Chemistry, University of Texas, Austin, TX 78702, USA.
*Corresponding author. Email: dave.thirumalai@gmail.com

RESULTS AND DISCUSSION

Kin1 binding elicits an asymmetric response between the plus- and minus-end tubulins

In an interesting experiment (*24*), it was observed that binding of Kin1 to MT is cooperative. Relative to a stationary Kin1 (achieved by coating Kin1 by fluorescent beads), which hydrolyzes ATP without stepping, a second Kin1 is more likely to bind to the plus end of the same MT (*24*). The effect of cooperative binding propagates up to distances on the order of about a few micrometers. This finding is unexpected because a single MT protofilament is essentially one-dimensional (1D), and all the interactions are short-ranged, which implies that long-range correlations are unexpected.

The experimental observations (*24*) raise the possibility that Kin1 binding to MT affects the fluctuations of the residues at the plus end differently from the residues at the minus end. To test this hypothesis, we constructed a protofilament consisting of four potential kinesin binding sites. We first calculated the amplitude of fluctuations of each MT residue using a structure without a bound Kin1. Next, we created a complex with a Kin1 dimer attached to the two middle binding sites in the MT segment, leaving free the binding sites at the plus and minus ends [referred to as $(Short)_1$-DU-Near complex; see Fig. 1A]. We then calculated the change in tubulin fluctuations at the minus end, δ_i^-, and the plus end, δ_i^+ (Materials and Methods). To determine whether there is an asymmetry in the response of a tubulin, we calculated $\Delta_i^R = \delta_i^- - \delta_i^+$ (Eq. 9). A nonzero value of Δ^R would imply that the two ends of the tubulin are affected differently upon Kin1 binding.

The black line in Fig. 1B shows the difference in tubulin response as a function of the α- and β-tubulin residues. The data show that (i) the asymmetric response is transmitted throughout the tubulin structure, and (ii) α and β domains within a single tubulin respond very differently. The residues that display the largest asymmetry are highlighted with big blue and red beads in Fig. 1C. These residues are clustered on the outside surface, next to the interdimer interfaces between the neighboring tubulin dimers. In contrast, residues that display less asymmetric responses (marked with smaller pink and cyan beads in Fig. 1C) are on the luminal side and the intradimer interface.

Next, we analyzed the changes in the MT dynamics induced by a Kin1 monomer, which is of particular interest because for processive motion, one of the heads has to be bound to the MT at all times (*1*, *2*, *25*–*29*). Thus, to study the effect of a dimeric motor that is in the middle of a step, we bound a single Kin1 head in the middle of an MT segment containing three binding sites. Depending on the state of the neck linker (NL), we refer to these constructs as $(Short)_1$-U-Near or $(Short)_1$-D-Near (Fig. 1A). We repeated our calculations to obtain Δ^R (Eq. 9). Just as found in $(Short)_1$-DU-Near, a single Kin1 motor domain also triggers asymmetric changes in the MT fluctuations with nonzero Δ^R values (orange and green lines in Fig. 1B). These calculations show that the plus and minus tubulin dimers respond asymmetrically to the presence of either a single Kin1 head or a Kin1 dimer in the middle binding site(s).

We then constructed a complex with three protofilaments $(Short)_3$-U-Near to investigate the effect of a bound Kin1 on different potential landing sites for the diffusing head (fig. S3). The response profile of the binding site that would correspond to a side step is clearly different and almost opposite to the response of the expected binding site.

Asymmetry in α- and β-tubulin dimer binding residues

To further analyze the dynamics of the MT residues that directly bind to Kin1 (listed in table S2 and highlighted in Fig. 2A), we plot in Fig. 2B their motilities with and without a bound motor domain for the $(Short)_1$-D-Near construct. A comparison of the responses shows a clear difference between the plus- and minus-end binding residues. For example, potential Kin1 binding sites on β-tubulin are more mobile at the plus end but are less so at the minus end. Conversely, the binding sites on α-tubulin are less mobile at the plus end but are more so at the minus end. Kin1 binding enhances these differences, showing clear asymmetric effects between the two ends. Since the residues involved in Kin1 binding are mainly positively charged, while the residues at the outer surface of the MT are predominantly negatively charged (15 negatively charged residues are shown in Fig. 2A) (*30*, *31*), it has been suggested that Kin1 diffuses along MT and docks to a particular binding site driven by favorable electrostatic interactions between α4 and the negative charges located in the β-tubulin (*32*). We observe enhanced flexibility at the plus end of the main Kin1 binding domain (H12 of β-tubulin), which could lead to a stronger binding affinity, implying that the plus end should have a stronger interaction with the diffusing head than the minus end.

Stresses generated by Kin1 binding expand the MT lattice

We next investigated the effect on the elasticity of the MT lattice (Eqs. 6 and 7) when Kin1 binds by comparing the correlation profiles $\langle \vec{R}_i \cdot \vec{R}_j \rangle$ and $\langle \vec{e}_i \cdot \vec{e}_j \rangle$ of tubulin dimers with (upper triangle matrix) or without Kin1 (lower triangle matrix) in Fig. 3 (A and B). The sequence of each tubulin is divided into three domains, highlighted in the 3D structures in Fig. 3 (C and D).

The correlation matrix, $\langle \vec{R}_i \cdot \vec{R}_j \rangle$, shows that Kin1 induces coordinated motion involving key residues within the tubulin dimers. First, two small black squares in Fig. 3A represent the effect of switching from anticorrelated motion, in the absence of Kin1, to positive correlation when Kin1 binds to MT between the C-terminal domains of the α- and β-tubulins (αC and βC) (see also Fig. 4B). Second, the enhancement in the correlations is greater within the N-terminal domain of the β-tubulin (βN versus βN, see the two connected magenta dash-dot triangles, the triangle below is greener). Third, the intermediate domain of the α-tubulin, without direct contacts with Kin1, becomes negatively correlated with the N-terminal domain of the β-tubulin (αI versus βN; see the two blue dashed rectangles).

The very act of Kin1 binding results in substantial conformational changes in the tubulin dimers, which results in the distortion of the MT lattice. In particular, Kin1 binding leads to a more stable β-tubulin and twisted α-tubulin, which is reflected in $\langle \vec{e}_i \cdot \vec{e}_j \rangle$ in Fig. 3B. In the absence of Kin1, there are no apparent alignments in the dimers, represented by patchy colors throughout the upper matrix. Upon Kin1 binding (lower matrix), the entire β-tubulin is aligned with each other (most values are green within the highlighted magenta dash-dot triangle in the lower matrix). The soft modes show that the motion is anticorrelated with the intermediate domain of the α-tubulin (most of the values are red in the highlighted blue dashed rectangles in the lower matrix).

These results are consistent with the previous observation that although β-tubulin is the primary binding site of Kin1, most differences between the cryo–electron microscopy (cryo-EM) data of MT coated with and without Kin1 are found in the αI domain of α-tubulin (*13*). Kin1 binding results in an increase in the mass near the center of the α-tubulin toward the binding interface of the adjacent tubulin dimer in (*13*). This increase in mass [marked with a red arrow in figure 6, A, F, and G, of (*13*)] is at the same location of the αI domain (marked with a red star in our Fig. 3D). From our calculations, the most

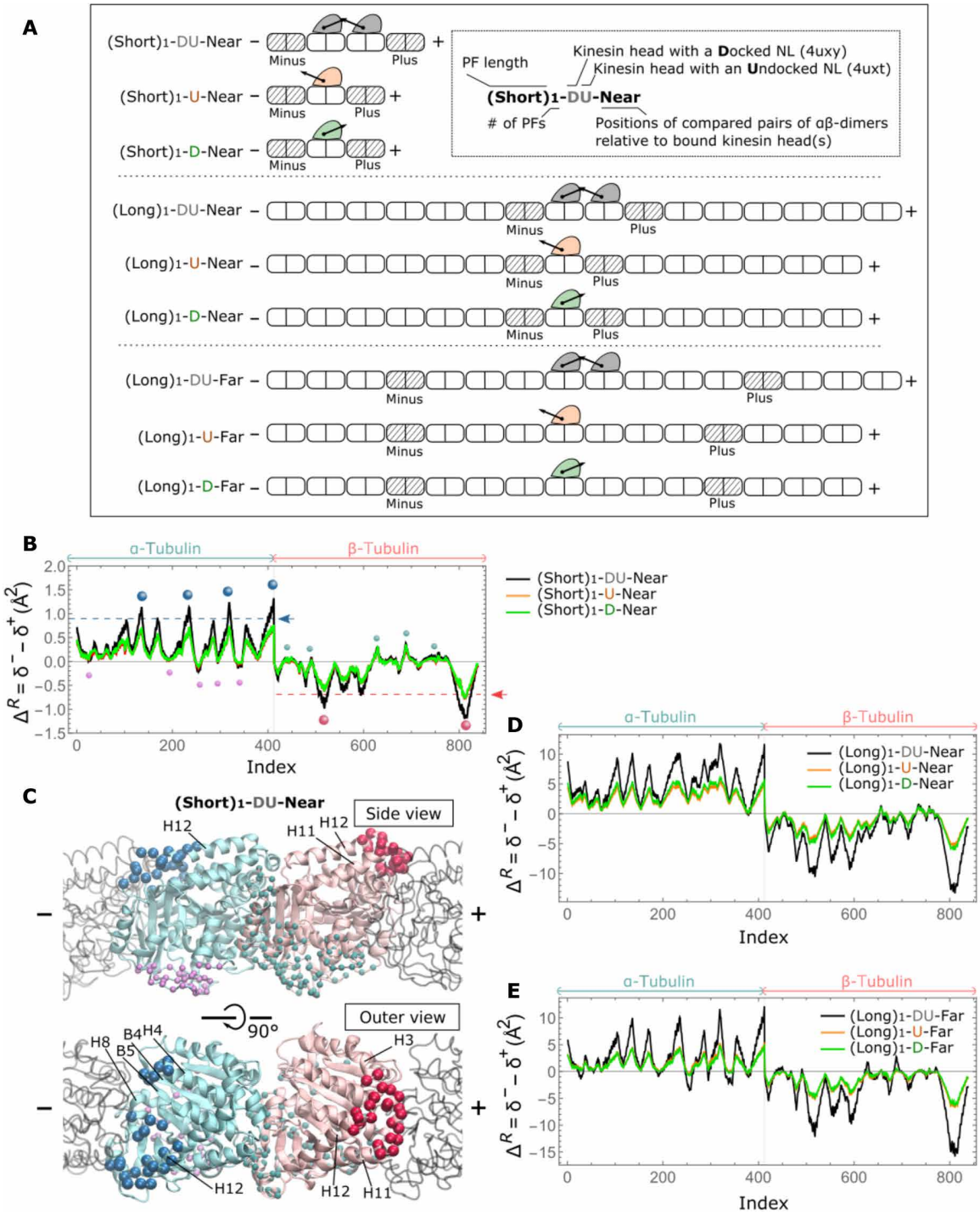

Fig. 1. Asymmetric response of the plus and minus ends of tubulin upon Kin1 binding. (**A**) Constructs used in the calculations. Each construct has one or two Kin1 motor domains (filled objects) bound to a short or long single protofilament consisting of multiple α/β-tubulin dimers (repeated opened objects). The docked (undocked) NL is represented as arrows pointing toward the plus (minus) ends of the protofilaments. The minus and plus α/β-tubulin dimers used to calculate the asymmetric response, Δ^R, are highlighted with stripes. Inset explains the labels. (**B**) Asymmetric response, Δ^R, calculated for the constructs with short protofilaments. Residues belonging to α- and β-tubulins are marked on top. Large spheres mark residues that show that Kin1 binding induces the largest asymmetric response in $(Short)_1$-DU-Near (residues with values in the black line above/below the dashed lines). Small spheres denote residues with the least asymmetric response (values closer to zero). These residues are visualized in 3D structure in (C). (**C**) Side and top views of the α-tubulin (blue) and β-tubulin (pink) within a protofilament (dark gray). Residues with the most asymmetric response are located at the outer surface near interdimer interfaces (large spheres). Residues with less asymmetric response are clustered at the luminal surface and intradimer interface (small spheres). (**D** and **E**) Δ^R, calculated for long protofilament constructs.

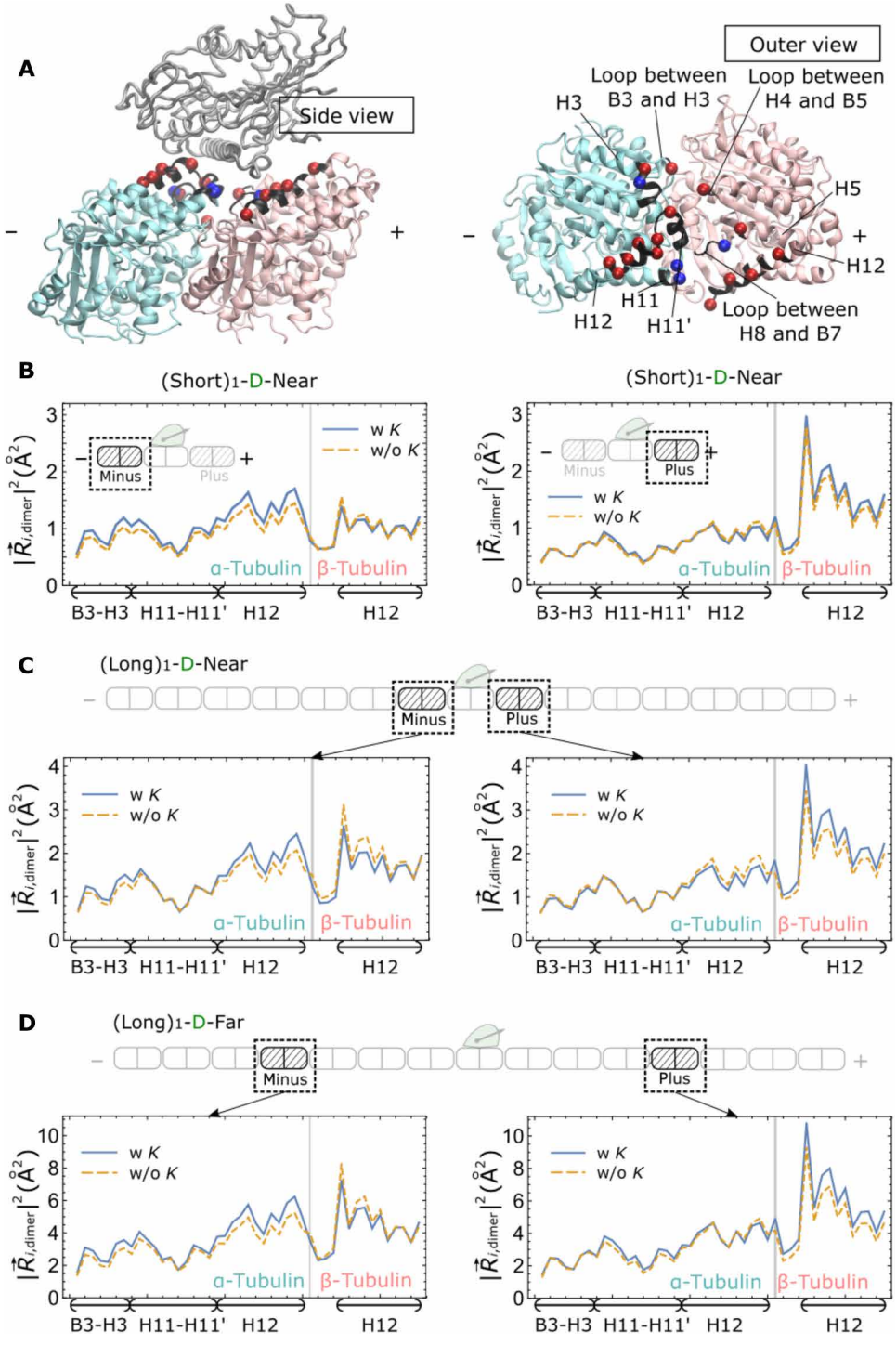

Fig. 2. Asymmetric response of Kin1 binding sites of plus- and minus-end tubulin. (**A**) Side view (left) and outer view (right) of the α-tubulin (light cyan) and β-tubulin (pink) structures with a bound Kin1 trailing head (gray). Potential Kin1 binding sites (listed in table S2) are highlighted in black, and their charges are shown in red (negative, 15 total) and blue (positive, 4 total). (**B** to **D**) Mobility relative to the center of mass of the corresponding dimer $|\vec{R}_{i,\mathrm{dimer}}|^2$ (Eq. 5) of potential binding sites at the minus end (left) and plus end (right) of the tubulin with (dashed line) and without (solid line) the bound Kin1 monomer in the $(\mathrm{Short})_1$-D-Near (B), $(\mathrm{Long})_1$-D-Near (C), and $(\mathrm{Long})_1$-D-Far (D) structures, respectively.

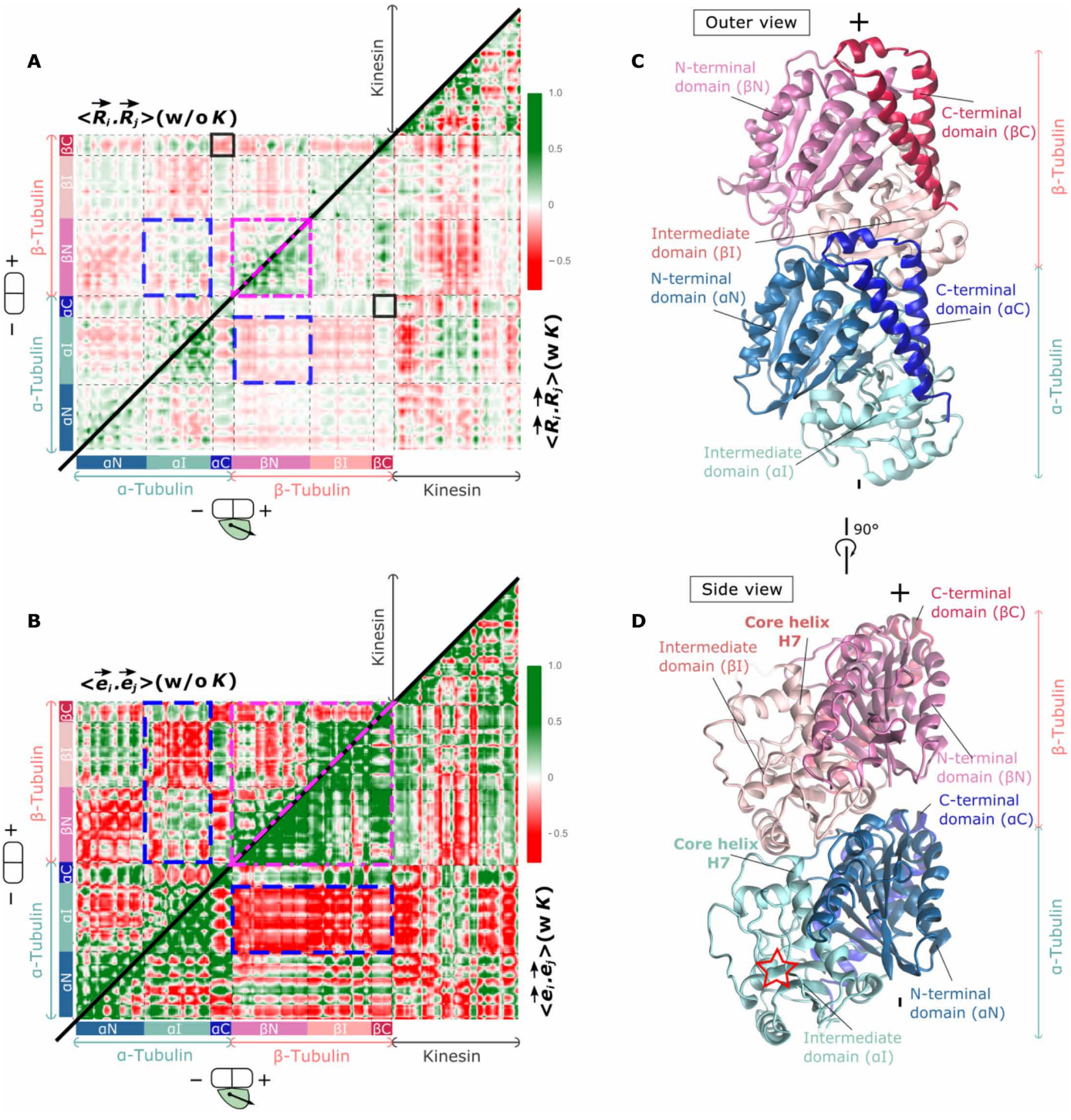

Fig. 3. Correlations between residues in tubulin before and after Kin1 binding. (**A**) Plots of spatial $\langle \vec{R}_i \cdot \vec{R}_j \rangle$ and (**B**) orientational $\langle \vec{e}_i \cdot \vec{e}_j \rangle$ correlation matrices for an α/β-tubulin dimer without a Kin1 (upper matrix, labeled top left corners) and with the bound trailing head (lower matrix, labeled side right corners). The plots are on the same color scale with green (red) representing positive (negative) correlation. Note that any value equal to or greater than 1 is shown in the darkest shade of green. Each tubulin has three domains (*35*): an N-terminal domain (αN or βN), an intermediate domain (αI or βI), and a C-terminal domain (αC or βC). The corresponding residues are marked as bars with different colors. Boxes with different colors highlight regions with maximum changes between the residues with and without bound Kin1. (**C**) Outer view and (**D**) side view of the α- and β-tubulin structure with different tubulin domains, colored corresponding to (A) and (B). A red star in (D) highlights the position of the αI domain, which is in the same position with the most increase in mass, detected in cryo-EM data upon Kin1 binding to the MT [figure 6 in (*13*)].

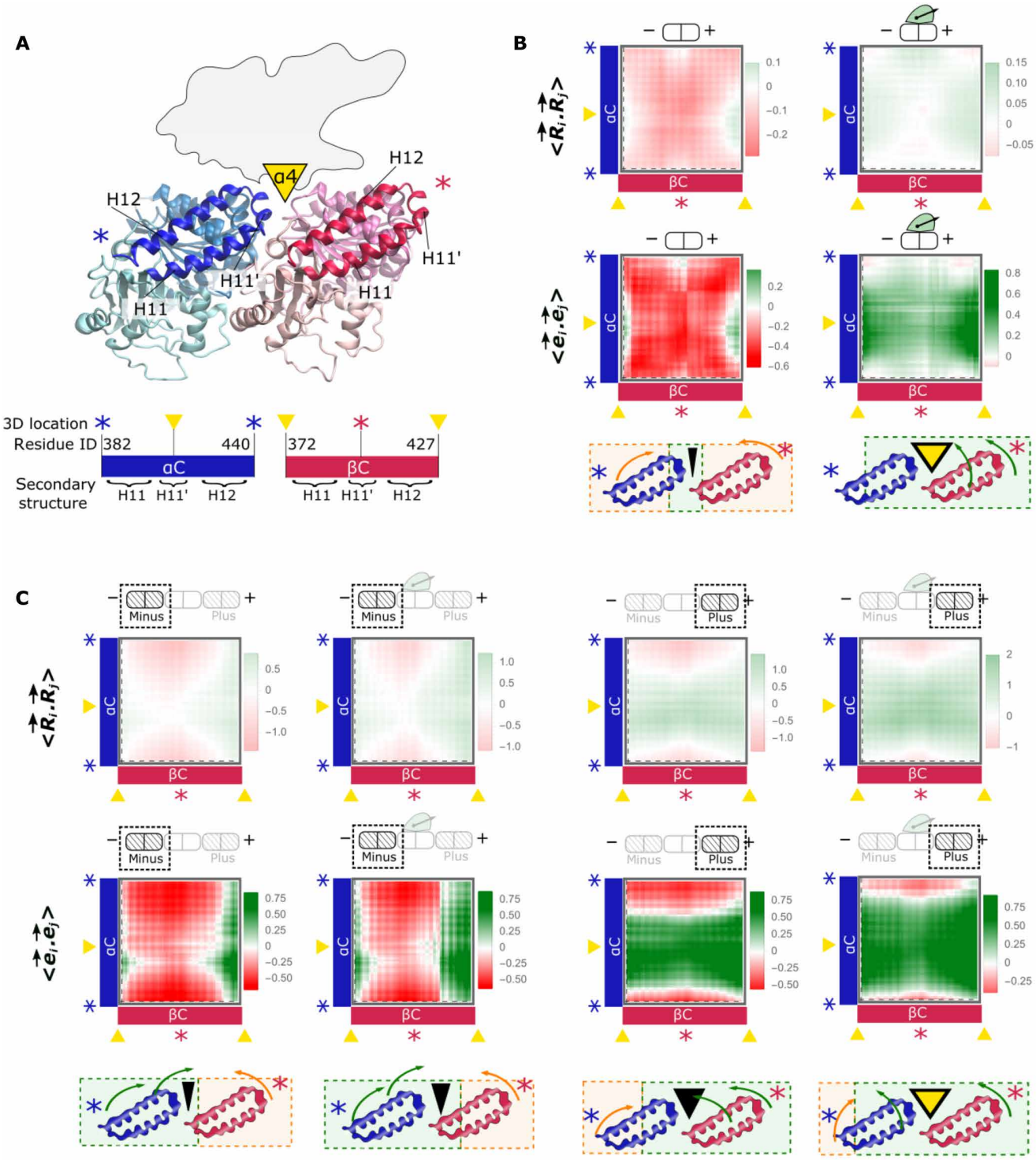

Fig. 4. Response of the outer surface of MT to Kin1 binding. (**A**) Top: Side view of a tubulin dimer with C-terminal domains of α- and β-tubulins (αC and βC, highlighted with darkest blue and red colors), consisting of H11, H11′, and H12 helices (*35*). Upon binding, helix α4 in Kin1 (shown as a yellow triangle) is between the two C-terminal domains and at the intradimer interface cleft. Bottom: Sequences of αC and βC are represented as blue and red bars, respectively. The locations of the residues near the intradimer and interdimer interfaces are marked with yellow triangles and stars, corresponding to the top figure. (**B**) Plots of $\langle \vec{R}_i \cdot \vec{R}_j \rangle$ (top) and $\langle \vec{e}_i \cdot \vec{e}_j \rangle$ (center) between C-terminal domains of an αβ-tubulin dimer in the absence of Kin1 (left) and with the bound trailing head (right). The plots are on the same color scale with green (red) representing positive (negative) values. Bottom: The positions of the residues with positive correlations are mapped to side views of corresponding C-terminal domains with dashed green boxes; the negative correlations are in orange boxes. (**C**) Similar to (B) but correlation matrices are calculated for minus- and plus-end tubulin dimers in the $(Short)_1$-D-Near construct.

notable effect of Kin1 is the anticorrelated fluctuations between the entire β-tubulin and the αI domain, which increases the mass due to colocalization in this region. Recent cryo-EM data on different types of MTs also show that changes in the MT lattice arise mainly due to the changes in α-tubulin (*33*, *34*). The negative correlation between the intermediate domain of α-tubulin and the β-tubulin means that the two parts undergo collective movement that oppose one another, which could distort the polar track. As a consequence, the MT lattice expands upon Kin1 binding (*14*, *15*).

Kin1 markedly alters the soft modes of the C-terminal domains of tubulin

We then focus on helices H11, H11′, and H12, classified as the "C-terminal domains" (*35*) (see also Fig. 4A). The C-terminal domains include several Kin1 binding sites (Fig. 2A) along with many residues that we identified earlier as having the largest values of Δ^R (see Fig. 1C). Figure 4B shows two distinct correlation profiles, $\langle \vec{R}_i \cdot \vec{R}_j \rangle$ (dynamic) and $\langle \vec{e}_i \cdot \vec{e}_j \rangle$ (orientation, see Materials and Methods). The C-terminal domains of the two tubulins are anticorrelated (red) when Kin1 is not bound, and they are correlated (green) when a Kin1 is bound. The two distinct profiles show that, upon binding, residues in the MT binding regions of kinesin become stiffer (see fig. S1) with α4 helix of Kin1 wedging into the cleft formed at the intradimer interface between the two C-terminal domains, keeping the cleft open (represented by a yellow triangle in Fig. 4B, right). On the other hand, when Kin1 is not bound, the cleft is empty, allowing anticorrelated soft modes to be dominant in the outer surface of tubulin, effectively closing the cleft. The two-state closed-to-open transition expands the MT lattice and creates the asymmetric response that sets the stepping directionality. Movie S1 shows the correlated versus anticorrelated motions in the first modes in the two states.

Kin1 opens a cleft at the α/β intradimer interface and enhances binding at the MT plus side

Having determined the distinct correlation profiles of the Kin1-bound and Kin1-free modes at the binding site itself, we tested the correlations at the adjacent binding sites as well. We expect that correlated motions between the C-terminal helices would increase the probability that additional Kin1s would bind to the plus-end tubulin since they keep the cleft open (referred to as OC), while anti-correlated movement that effectively closes the cleft (CC) would decrease the binding probability. We calculated the correlation profiles of the plus and minus ends binding sites when Kin1 is absent as well as when it is bound to the middle binding site of the $(Short)_1$-D-Near structure. The right and left sides of Fig. 4C profiles are markedly different at the plus and minus ends of the MT. In particular, upon Kin1 binding, the correlation profiles of the plus-end binding site (the rightmost column of Fig. 4C) are similar to the profiles of the tubulin-Kin1 complex in Fig. 4B. Although Kin1 binding extends the correlated region in the C-terminal domains of the minus-end tubulin dimer, their motions remain mostly anticorrelated, suggesting that the cleft between the two dimers is effectively closed.

The relative correlations between the residues adjacent to the cleft determine Kin1 binding affinity. In the region of an MT that is on the plus side of an already bound Kin1, the clefts are correlated and effectively open with a high affinity for Kin1 binding. Thus, the probability of the cleft being open to the right (plus end of the MT) of bound Kin1 is higher than in the minus end, which is a cooperative effect that propagates (see below).

Asymmetric plus and minus response is a long-range effect

To investigate whether the propensity for the cleft in the OC state, poising another Kin1 to bind, can be sustained over long distances, we tested the effect of a bound Kin1 monomer and dimer on the MT dynamics by incorporating larger MT segments in constructs shown in Figs. 1 (D and E) and 2 (C and D). In all cases, the dynamic responses of the MT were alike. Unexpectedly, there is an enhanced probability for the tubulin dimers in the plus end of a bound Kin1 to be in the OC state compared to the minus end. The cooperative transition from Kin1-induced CC → OC persists even several tubulin dimers to the plus end of the location of the bound Kin1 (Fig. 1E). Because of the two-state closed-to-open transition, the long-range strain-induced asymmetric response of the MT to Kin1 binding could occur in a 1D lattice even if the interactions are short-ranged.

MT binding induces correlations within the nucleotide binding sites in the motor

So far, we have only considered the changes in the MT dynamics and structures in the α/β-tubulin upon Kin1 binding. It is appreciated that the MT has a profound effect on the steps in the catalytic cycle of the motor. For instance, MT enhances ADP release rate by nearly a factor of 1000 (*12*). In addition, it has been proposed that cooperative motion of switches I and II is necessary for many steps in the biochemical cycle (*36*, *37*). We tested the possibility that binding to MT induces correlated response in the relative dynamics of switches I and II, along with ADP and its binding sites, which might provide a partial explanation for the substantial ATPase rate changes.

To assess the changes in the fluctuations of switches I and II, we analyzed the correlations between the switches for a kinesin bound to an MT and for the unbound motor. We used the 30 lowest energy normal modes of an ADP-bound monomeric kif1a [1i5s.pdb (*38*)] and an ADP-bound kif1a-MT complex [2hxh.pdb (*39*)]. For both the structures, we calculated the average dynamic correlations, $\langle \vec{R}_i \cdot \vec{R}_j \rangle$, between all the pairs of residues in switches I and II (Eq. 6 in Materials and Methods). Figure 5A compares the two correlation matrices for MT-bound kinesin (bottom) versus the unbound motor (top, plotted with the same color scale as the bottom). A greater value with darker green indicates an increase in correlation between a given pair of residues in the switches. There is a remarkable difference in $\langle \vec{R}_i \cdot \vec{R}_j \rangle$ with and without MT. There is a significant increase in the correlations upon MT binding for all the residue pairs, with almost the entire matrix becoming nearly dark green (compare the bottom to the top in Fig. 5A). For example, binding to an MT enhances the correlations between the fluctuations of kinesin residues R216 and E253 (highlighted in the black boxes) by a factor of ≈5.

There are two independent factors that might contribute to the enhancement in the correlated motions reflected in $\langle \vec{R}_i \cdot \vec{R}_j \rangle$ in the presence of the MT: (i) the increase in the spatial fluctuations and (ii) directional alignment in the residue motions. To isolate these effects, we calculated the average orientational correlations $\langle \vec{e}_i \cdot \vec{e}_j \rangle$ between all pairs of switch I and switch II residues (Eq. 7). Figure 5B (plotted with the same color scale) shows the directional correlation matrices in the two cases. Almost all the values in the matrix plotted for MT-bound kinesin are larger (darker green color in Fig. 5B, bottom) than for apo-kinesin (Fig. 5B, top), indicating that the fluctuations in the two switches are orientationally aligned upon binding to MT. The correlations between residues R216 and E253 (black boxes) increase by a factor of 2 upon MT binding. Comparisons of the results in the two panels in Fig. 5B show that the extent of alignment

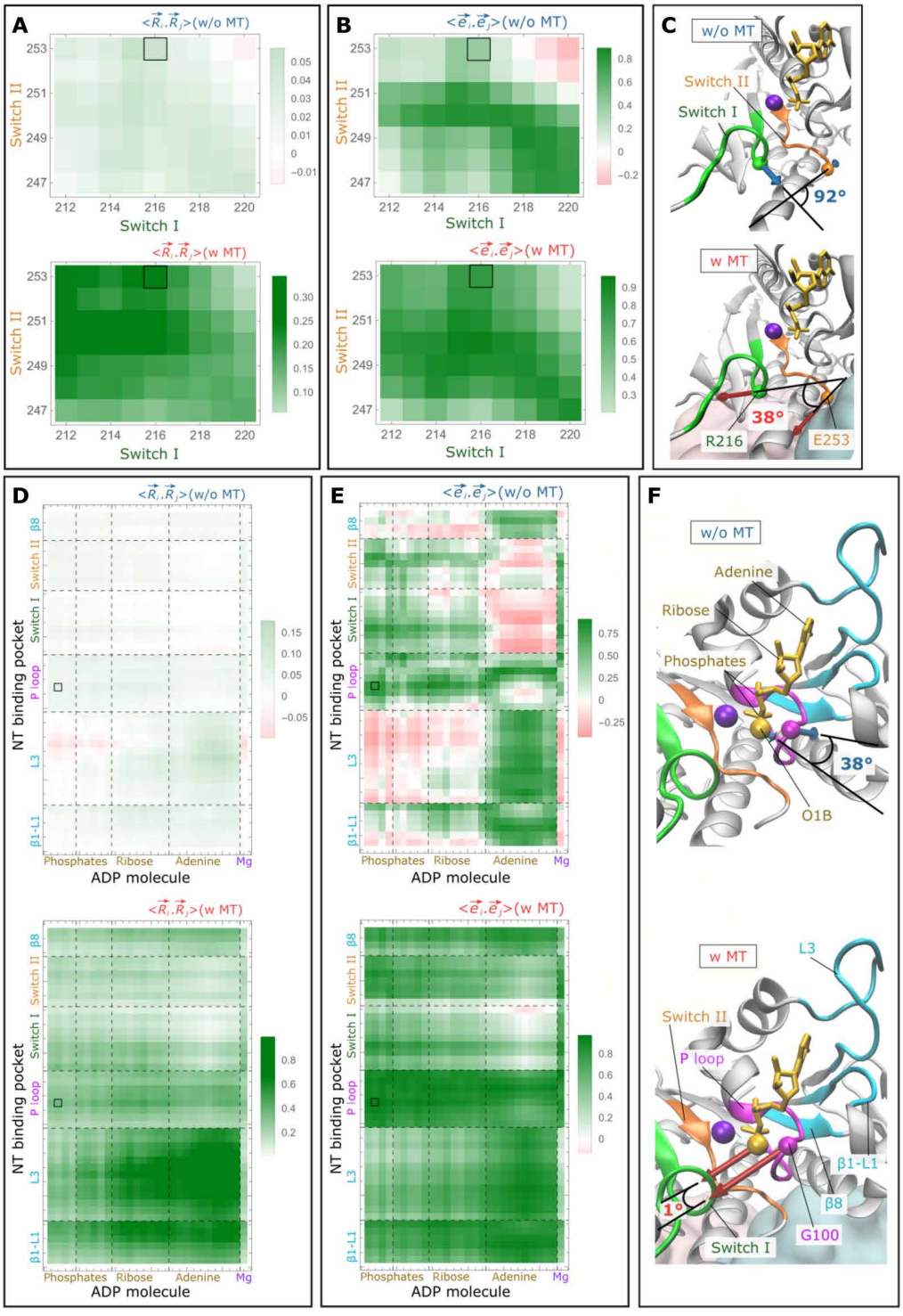

Fig. 5. MT binding induces correlated translational and directional movements between switch I and switch II and between ADP and its binding site. (**A**) Spatial $\langle \vec{R}_i \cdot \vec{R}_j \rangle$ and (**B**) orientational correlation matrices $\langle \vec{e}_i \cdot \vec{e}_j \rangle$ (labeled on the top right corners) between switches I (residues 212 to 220) and II (247 to 253) for the unbound kinesin 1i5s.pdb (top) and the MT-bound kinesin 2hxh.pdb (bottom). Positive (negative) correlation is shown in green (red) hue (scale bars on the right). (**C**) Structures of switch I (green) and switch II (orange) relative to ADP molecule (yellow) and Mg^{2+} ion (purple) in the unbound (top) and bound structures (bottom). α/β-Tubulins are in light cyan and pink. Residues R216 (switch I) and E253 (switch II), marked with stars in the 1i5s sequence in fig. S1D, are represented as green and orange beads at the C_α atoms. The angle measures the relative motion of the lowest mode (arrows) between the two residues. (**D**) to (**F**) are similar to (A) to (C) but for correlations between ADP molecule (yellow), Mg^{2+} ion (purple), and the ADP binding site (color-coded accordingly). Residue G100 of the P loop (magenta star in fig. S1D) and O1B atom of the ADP molecule are represented as yellow and magenta beads at their α carbon atoms, respectively.

of the switches I and II, as measured by $\langle \vec{e}_i \cdot \vec{e}_j \rangle$, increases when the motor binds to the MT. In Fig. 5B, the bottom panel shows that the residues in the two switches exhibit a high degree of orientational correlation with complete absence of anticorrelation, observed in the upper right corner in the top panel.

To visualize the changes in the movements of the two switches, we plot in Fig. 5C the lowest energy eigenvectors associated with residues R216 and E253 of the isolated kinesin and the MT-bound kinesin. For an unbound motor (top) the eigenvectors of the pair are almost perpendicular. In contrast, upon binding to an MT (bottom), the same residues are aligned with each other—the relative angle of the first eigenvectors changes from 92° to 38° accompanied by increased fluctuations. Together, these results show that interactions with the MT produces correlated responses in key structural elements in the motor domain.

Switches I and II are thought to play an important role in positioning the critical water molecule that ruptures the phosphodiester bond of the γ-phosphate of ATP during the hydrolysis process. Originally proposed for myosin (*40*), the arrangement of the water molecule relies on the formation of a salt bridge between the conserved arginine in switch I and the conserved glutamic acid in switch II (R216 and E253 in kif1a). The formation of the salt bridge is also important for the MT-stimulated ATPase activity of kinesins (*41*–*43*), including other kinesin-related kar3 (*44*) and ncd (*45*) motors. Although the calculations based solely on ENM cannot account for the formation and rupture of salt bridge, the observed increase in the correlated fluctuations between R216 and E253 suggests that the salt bridge formation could be a contributing factor in the enhanced ATP hydrolysis and ADP release rates from the motor head.

To obtain additional insights into the increase in the ADP release, we analyzed the correlations using $\langle \vec{R}_i \cdot \vec{R}_j \rangle$ between the fluctuations in the nucleotide and the residues in the binding pocket. Comparing the correlations calculated using an MT-bound and an unbound kinesin in Fig. 5D, we find that most of the values in the bottom panel of Fig. 5D are greater (represented in dark green) than in the top panel, indicating an increase in the dynamic correlations upon MT binding.

The increase in $\langle \vec{R}_i \cdot \vec{R}_j \rangle$ upon binding to MT is caused by an increase in the magnitude of the fluctuations, as well as an increase in the orientational correlations $\langle \vec{e}_i \cdot \vec{e}_j \rangle$. The results in Fig. 5E, showing the relative changes in the directional correlations upon MT binding, establish that binding to the MT induces alignment in the fluctuations of the nucleotide binding pocket and the ADP molecule. Without MT, different structural components of the ADP molecule show opposite fluctuations with parts of the binding pocket that do not directly interact with each other. For instance, adenine does not directly interact with the switches (see Fig. 5F), and they have negative $\langle \vec{e}_i \cdot \vec{e}_j \rangle$ values (represented in red hue in Fig. 5E, top). Similarly, Mg^{2+} ion, ribose, and phosphate are far from L3 (see Fig. 5F), and they also have negative $\langle \vec{e}_i \cdot \vec{e}_j \rangle$ values (red hue in Fig. 5E, top). However, upon MT binding, ADP is aligned with the whole nucleotide binding site, as shown by the green hue in Fig. 5E (bottom). Hence, MT binding results in the entire nucleotide binding sites to fluctuate in unison, which could explain the faster release of ADP.

As switches I and II harbor the Mg^{2+} ion and the γ-phosphate, another conserved motif, normally referred to as the P loop, stabilizes the α- and β-phosphates of the nucleotide molecule. To illustrate the ADP fluctuations, we considered the correlations between residue G100 in the P loop and ADP phosphate atom O1B. We highlighted their values with black boxes in Fig. 5 (D and E) and illustrate their first nonzero eigenvectors in Fig. 5F. After binding to MT, the amplitudes of fluctuations increase more than threefold in both G100 and O1B. In addition, there is enhanced directional alignment (Fig. 5F, bottom versus top). We surmise that MT binding substantially alters the local dynamics of the nucleotide binding pocket by making the constituent residues fluctuate with larger amplitude along the same direction.

We also calculated the $\langle \vec{R}_i \cdot \vec{R}_j \rangle$ and $\langle \vec{e}_i \cdot \vec{e}_j \rangle$ between AMPPNP (sdenylyl-imidodiphosphate) and the binding pocket before and after MT binding. We found that, just as is the case for ADP binding, both $\langle \vec{R}_i \cdot \vec{R}_j \rangle$ and $\langle \vec{e}_i \cdot \vec{e}_j \rangle$ between AMPPNP and the binding pocket increase upon MT binding. It is possible that the increase in the correlation between the fluctuations of ATP and its binding pocket contributes to an increase in ATP hydrolysis rate upon MT binding (*46*).

These findings are consistent with two experimental observations. First, a recent structural study (*47*) shows that Mg^{2+} inhibits ADP release in kif1a and that the fluctuations (measured by *B* factors) of ADP increase during Mg^{2+} release. The increase in the fluctuations of ADP upon MT binding, found here, may similarly correlate with the rate increase in ADP release enhancement. Second, EPR spectroscopy of spin-labeled ADP (*48*) showed that the relative angular motions (as measured by a cone angle) between ADP and its binding pocket decrease upon MT binding. This is in accord with our finding that the directional correlation, $\langle \vec{e}_i \cdot \vec{e}_j \rangle$, between ADP and the associated binding pocket increases upon MT binding, which is manifested as a decrease in the cone angle.

Reciprocal interactions between kinesin and MT, processivity, and ADP release

The asymmetric response of the tubulin at the plus and minus ends of the MT, expansion of the mechanical stress–induced MT lattice, and the CC → OC transition lead to a conceptual model that we illustrate in Fig. 6. The expansion of the MT lattice, accompanied by the formation of the OC state in which the fluctuations in the β domain are enhanced, propagates preferentially toward the plus end of the MT. The consecutive formation of the OC states to the right (toward the plus end of the MT) of a bound Kin1 (schematically indicated by the green region in Fig. 6) leads to preferential binding of additional Kin1s toward the plus end. The same picture holds when only a single motor, which is most commonly studied in in vitro single molecule experiments, walks processively on the MT. In this case, when Kin1 binds, it induces multiple CC → OC transitions in the tubulin dimers that are at the plus end. When the trailing head detaches and diffusively searches for the subsequent binding site, it is more poised to bind to the OC than to the CC state, which would ensure processivity. Thus, it is the mechanical stress–induced formation of the OC states, which although occurs within a single α/β-tubulin but has a long-range effect, that explains both the directionality and processivity of kinesin motors. Conversely, α/β-tubulin alters the motor dynamics, especially at the nucleotide binding sites (Fig. 5), which likely facilitates the release of ADP.

Here, we specifically focus on the interactions between kinesin and MT, how MT dynamics affects the stepping of the motor, and how, in return, the motor affects the internal dynamics of MT. Here, we pieced together related tubulin and different MT-bound Kin1 structures, along with MT-bound kif1a and MT-free kif1a structures with ADP to create models in various states. The residue-dependent mechanical responses show that the interface between the MT and

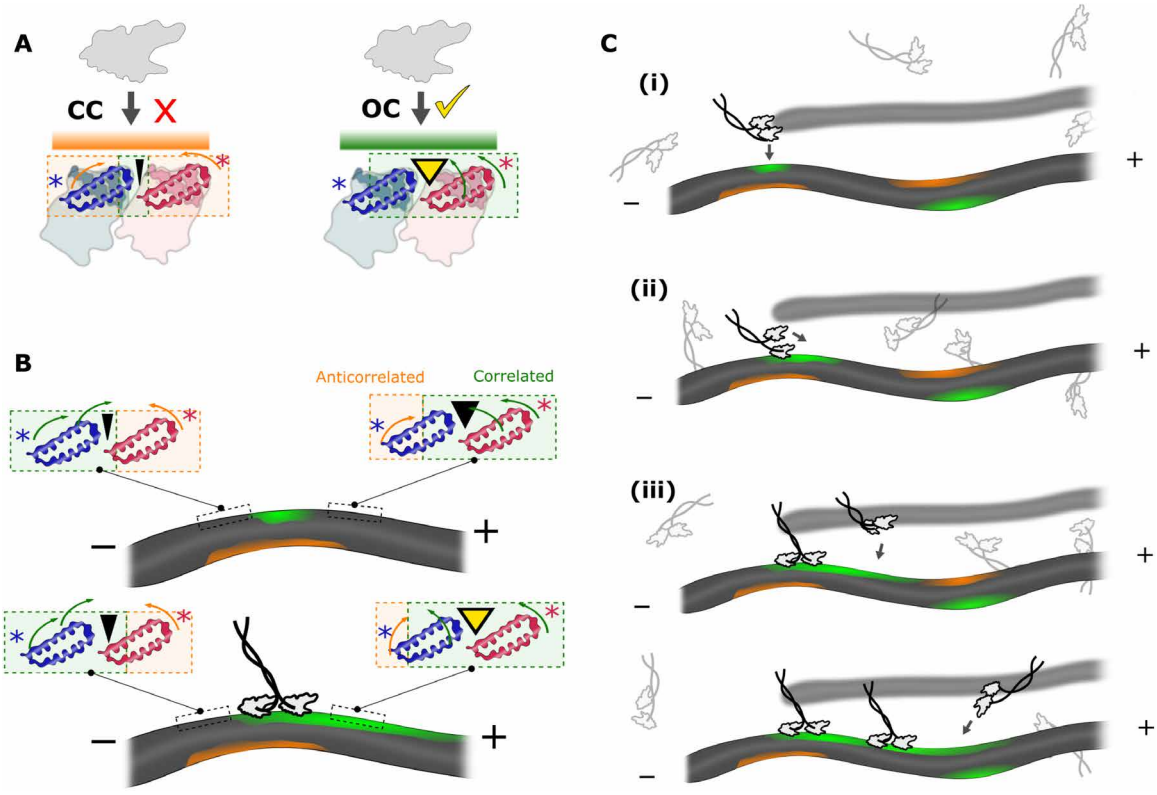

Fig. 6. Emerging model summarizing the asymmetric response. (**A**) Two soft modes: (left) anticorrelated movements between the two C-terminal domains close the cleft at the intradimer αβ interface (CC), inhibiting Kin1 binding; (right) correlated movements across the entire Kin1 binding site enable the docking of the α4 helix into the stress-induced open cleft (OC). (**B**) Kin1 binding induces correlated soft modes (OC states, green) in the plus-end direction for other motor head(s) to bind with high probability. (**C**) Predicted effects inside cells. (i) Initial Kin1 binds with high probability to OC sites (green). Examples of those OC regions are at the convex side of a bent MT (*15*). (ii) As Kin1 walks, the bound head switches the adjacent binding site at the plus end to an OC state, favoring hand-over-hand landing of the diffusing head. (iii) A bound Kin1 dimer induces correlated soft modes (green) toward the plus end, attracting additional motors to bind to the plus end of the same MT (*24*). This creates a cooperative effect that promotes other motors to land on the same MT while avoiding neighboring MTs (blur MT in the background) at nonsaturated Kin1 concentrations (*23*).

the motor stiffens upon binding, which, in turn, allosterically alters the proximal nucleotide binding sites. The MT induces correlations between switch I and switch II and ADP by aligning the binding sites along a preferred orientation. The internal dynamics of the motor as well as the MT track reveal that interaction between Kin1 and the MT produces long-range (possibly across the whole length of the MT) allosteric effects that govern the reciprocal dynamic relationship between MT and the motor.

The most important finding of this work is that the plus and minus ends of the MT respond asymmetrically to Kin1 binding to a specific α/β-tubulin dimer. Unexpectedly, the asymmetry persists over a long spatial range, which is made possible because Kin1 induces stress-induced closed (CC) to open (OC) transition in the cleft of the α/β C-terminal domains, the binding site of the motor. The CC → OC transition also expands the MT lattice (*14*, *15*), presumably downstream of the site of the bound motor. The accessible kinesin binding sites in the front and rear ends of α/β-tubulin produce asymmetric mobility patterns (Fig. 2). The dominant soft modes of the MT-Kin1 complex result in the binding site being correlated, which persists on the plus side of the MT but not on the minus side (Figs. 4 and 6, A and B). Thus, the inherent bias in the stepping toward the plus end of the MT is encoded in the strain-induced change in the affinity of the motor for sites on the α/β dimer. This principal finding, whose origin is mechanical in nature, rationalizes the experimental observation (*24*) in structural terms. It implies that binding of an individual motor induces long-range correlations in the MT lattice (*24*, *49*), which leads to preferential binding of kinesin at sites to the plus end of an already bound motor.

Our calculations also show that Kin1 induces positive correlations within the β-tubulin, its primary binding monomer, and anticorrelations between the β-tubulin and the intermediate domain of α-tubulin, the αI domain (Fig. 3). This is in excellent agreement with the cryo-EM (*13*). The recent cryo-EM data (*34*, *50*) observed that the MT lattice can be in two different states, with the guanosine 5′-diphosphate (GDP)–MT lattice being more compact than the GMPCPP-MT (guanosine-5' [(α,β]-methyleno] triphosphate) lattice. The expansion/compaction arises from the rearrangement of the αI domain, which is in accord with our calculations. Furthermore, it has been shown that Kin1 can expand the compact GDP-MT lattice (*14*, *15*), suggesting that the Kin1-bound GDP-MT structure should have a higher pitch distance closer to the GMPCPP-MT lattice state in solutions.

We interpret the origin of the CC → OC transition, which is linked to the MT expansion, to the marked alterations in the soft modes within the tubulin dimers. This affects the intermediate domain αI to move in an anticorrelated manner relative to the entire β-tubulin. These highly anticorrelated modes redistribute the mass

inside α-tubulins (*13*), thus effectively expanding the GDP-MT lattice in solution (*14*, *15*). The extensive dynamic interplay between the motor and MT shows that MT should be thought of as an active and dynamic material. The most important conclusion from our study is that it is the interplay of the conformational dynamics involving both kinesin and the tubulin dimers that sets the stepping direction. This results in anisotropic response in tubulin when kinesin binds, which could propagate in an asymmetric manner throughout the MT lattice.

MATERIALS AND METHODS

Elastic network model

Native proteins undergo correlated movements, which control many functional aspects. A number of studies have shown that these movements depend predominantly on the shape of the protein. This is the main reason why analysis of normal modes has been successful in capturing the intrinsic motions of a number of proteins, including tubulins and kinesins, the focus of our study. We model kinesin and MT as networks composed of N nodes with each residue representing a single node, located at the position of its C_α atom. In the calculations with explicit ADP (AMPPNP), each nucleotide heavy atom is also taken to be a node. Two nodes, *i* and *j*, are connected by a harmonic spring if the distance between them in the PDB structure is less than R_c = 10 Å. We have verified that changing the cutoff distance over a reasonable range up to R_c = 8 Å does not qualitatively alter the results.

The potential energy function for the elastic network is (*20*–*22*)

$$E = \frac{1}{2}\sum_{i,j:d_{ij}^0<R_c}\gamma\,(d_{ij}-d_{ij}^0)^2 \tag{1}$$

where γ is the spring constant that defines the energy scale (we set to be one unit), d_{ij} is the instantaneous distance between residues *i* and *j*, and d_{ij}^0 is the corresponding PDB distance, which is assumed to be the equilibrium separation. The dynamics of the system around the equilibrium state (the PDB structure) is determined from the normal modes, which are calculated by diagonalizing the Hessian matrix **H** obtained from the second derivatives of the internal energy in Eq. 1. The eigenvalues of the matrix, λ_m, correspond to the energies of the system, and the fluctuations of the modes are calculated from the corresponding eigenvectors q_m. The eigenvectors can be expressed in terms of the Cartesian components of the fluctuations of individual residues as

$$q_m = (\vec{R}_{1,m}, \vec{R}_{2,m}, \ldots\ldots, \vec{R}_{N,m}) \tag{2}$$

where $\vec{R}_{i,m}$ are the (*x*, *y*, *z*) components of the *i*th residue in motion.

In practice, we used 30 lowest-energy normal modes in our calculations. Our results remained unchanged when we increased the number of modes (see the Supplementary Materials).

Local stiffness, correlations between residues, and MT response

To determine the local stiffness, κ_i, we used the SPM (*18*, *19*). The SPM is used to probe the response of all the residues in response to a local perturbation at a specific residue. Within the ENM (Eq. 1), the local perturbation is realized by changing the value of γ. The perturbation alters the elastic energy in the normal modes. We define the local stiffness, κ_i, as the fraction of the effective elastic energy (SPM) stored in the *i*th residue over the residue fluctuation amplitude squared (the mobility), which turns out to be

$$\kappa_i = \frac{\langle \delta\omega_i \rangle}{\langle \vec{R}_i^2 \rangle} \tag{3}$$

where the mobility $|\vec{R}_i| \equiv \sqrt{\langle \vec{R}_i^2 \rangle}$ of a residue is

$$|\vec{R}_i|^2 = \sum_{m(\lambda_m\neq 0)} \frac{1}{\lambda_m}\vec{R}_{i,m}^2 \tag{4}$$

and $\langle \delta\omega_i \rangle = \sum_{m(\lambda_m\neq 0)} \frac{1}{\lambda_m}\delta\omega_{i,m}$, where $\delta\omega_{i,m}$ is the SPM response of residue *i* at mode *m*. The residue-dependent alterations in the stiffness and their locations in the structures are illustrated in fig. S1.

To separate the fluctuations of residues in a dimer from the dominant global movement, we determined the global mode of dimer *d* as $\vec{R}_{d,m} = \langle \vec{R}_{i,m} \rangle_{\text{dimer}_d} = \frac{1}{N_{\text{dimer}_d}} \sum_{i\in \text{dimer}_d} \vec{R}_{i,m}$, where N_{dimer_d} is the number of residues in dimer *d*. The motility of a given residue relative to the center of mass of the corresponding dimer is

$$|\vec{R}_{i,\text{dimer}_d}|^2 = \sum_{m(\lambda_m\neq 0)} \frac{1}{\lambda_m}(\vec{R}_{i,m} - \vec{R}_{d,m})^2 \tag{5}$$

We define the average dynamic correlation between residues *i* and *j* as

$$\langle \vec{R}_i \cdot \vec{R}_j \rangle = \sum_{m(\lambda_m\neq 0)} \frac{1}{\lambda_m}\vec{R}_{i,m} \cdot \vec{R}_{j,m} \tag{6}$$

where ⟨…⟩ implies an average, ideally taken over all the modes. Here, we use the first 30 lowest modes, which are the most dominant. We used the phrase "dynamic correlation" to distinguish it from "orientational correlation," which can be calculated using

$$\langle \vec{e}_i \cdot \vec{e}_j \rangle = \frac{\sum_{m(\lambda_m\neq 0)} \frac{1}{\lambda_m} \frac{\vec{R}_{i,m}\cdot\vec{R}_{j,m}}{|\vec{R}_{i,m}|\,|\vec{R}_{j,m}|}}{\sum_{m(\lambda_m\neq 0)} \frac{1}{\lambda_m}} = \frac{\vec{R}_i \cdot \vec{R}_j}{|\vec{R}_i|\,|\vec{R}_j|} \tag{7}$$

The dynamic response, δ_i^+, of a plus-end MT residue to kinesin binding is defined as

$$\delta_i^+ = \langle \vec{R}_i^2 \rangle_{wK} - \langle \vec{R}_i^2 \rangle_{w/o\,K} \tag{8}$$

where w *K* (w/o *K*) is calculated with (without) the bound kinesin, and the superscript refers to the plus end of the MT. The minus-end response, δ_i^-, can be similarly defined. The asymmetric nature of the response can be assessed using

$$\Delta_i^R = \delta_i^- - \delta_i^+ \tag{9}$$

Δ_i^R along with $\delta_i^\pm$ have units of [Å^2]. If the response of MT to kinesin binding is symmetric, then Δ^R in Eq. 9 would be zero, which implies that a nonzero value would indicate an inherent asymmetric response.

Kin1 dimer and MT structure preparation

The Kin1-MT protofilament structure preparation consisted of several steps, which are similar to the procedure described elsewhere (*7*). First, we extracted a protofilament structure from the structure of a segment of the MT (*51*). We augmented the filament with additional αβ-tubulin [1jff.pdb (*35*)] segments as needed. Next, we docked the

two new kinesin-tubulin structures provided in the PDB structures [4uxy and 4uxt (*52*)] to two adjacent binding sites on the MT filament so that the relative positions of the kinesins on the tubulin were similar to the solved kinesin-tubulin complexes. The leading head has a disordered NL and the trailing head has a docked NL. We repeated our calculations with an averaged equilibrium structure of the dimer (with full NLs) bound to the MT obtained in our previous study (*7*), obtaining similar results, thus establishing the robustness of the calculations. For the construct of single kinesin head bound with docked or undocked NL to α/β-tubulin heterodimer, we used either one of the two PDBs (4uxy or 4uxt).

SUPPLEMENTARY MATERIALS

Supplementary material for this article is available at https://science.org/doi/10.1126/sciadv.abn0856

View/request a protocol for this paper from *Bio-protocol*.

REFERENCES AND NOTES

1. S. M. Block, Kinesin motor mechanics: Binding, stepping, tracking, gating, and limping. *Biophys. J.* **92**, 2986–2995 (2007).
2. R. D. Vale, R. A. Milligan, The way things move: Looking under the hood of molecular motor proteins. *Science* **288**, 88–95 (2000).
3. A. B. Kolomeisky, M. E. Fisher, Molecular motors: A theorist's perspective. *Annu. Rev. Phys. Chem.* **58**, 675–695 (2007).
4. E. L. F. Holzbaur, Y. E. Goldman, Coordination of molecular motors: From in vitro assays to intracellular dynamics. *Curr. Opin. Cell Biol.* **22**, 4–13 (2010).
5. M. L. Mugnai, C. Hyeon, M. Hinczewski, D. Thirumalai, Theoretical perspectives on biological machines. *Rev. Mod. Phys.* **92**, 025001 (2020).
6. S. C. Ems-McClung, C. E. Walczak, Kinesin 13s in mitosis: Key players in the spatial and temporal organization of spindle microtubules. *Semin. Cell Dev. Biol.* **21**, 276–282 (2010).
7. Z. Zhang, D. Thirumalai, Dissecting the kinematics of the kinesin step. *Structure* **20**, 628–640 (2012).
8. J. W. Hammond, D. Cai, K. J. Verhey, Tubulin modifications and their cellular functions. *Curr. Opin. Cell Biol.* **20**, 71–76 (2008).
9. K. Tokuraku, M. Kuragano, T. Q. P. Uyeda, Long-range and directional allostery of actin filaments plays important roles in various cellular activities. *Int. J. Mol. Sci.* **21**, 3209 (2020).
10. R. A. Cross, Microtubule lattice plasticity. *Curr. Opin. Cell Biol.* **56**, 88–93 (2019).
11. J. C. M. Meiring, B. I. Shneyer, A. Akhmanova, Generation and regulation of microtubule network asymmetry to drive cell polarity. *Curr. Opin. Cell Biol.* **62**, 86–95 (2020).
12. D. D. Hackney, Kinesin ATPase: Rate-limiting ADP release. *Proc. Natl. Acad. Sci. U.S.A.* **85**, 6314–6318 (1988).
13. A. Krebs, K. N. Goldie, A. Hoenger, Complex formation with kinesin motor domains affects the structure of microtubules. *J. Mol. Biol.* **335**, 139–153 (2004).
14. T. Shima, M. Morikawa, J. Kaneshiro, T. Kambara, S. Kamimura, T. Yagi, H. Iwamoto, S. Uemura, H. Shigematsu, M. Shirouzu, T. Ichimura, T. M. Watanabe, R. Nitta, Y. Okada, N. Hirokawa, Kinesin-binding-triggered conformation switching of microtubules contributes to polarized transport. *J. Cell Biol.* **217**, 4164–4183 (2018).
15. D. R. Peet, N. J. Burroughs, R. A. Cross, Kinesin expands and stabilizes the GDP-microtubule lattice. *Nat. Nanotechnol.* **13**, 386–391 (2018).
16. Z. Zhang, Y. Goldtzvik, D. Thirumalai, Parsing the roles of neck-linker docking and tethered head diffusion in the stepping dynamics of kinesin. *Proc. Natl. Acad. Sci. U.S.A.* **114**, E9838–E9845 (2017).
17. S. Triclin, D. Inoue, J. Gaillard, Z. M. Htet, M. E. DeSantis, D. Portran, E. Derivery, C. Aumeier, L. Schaedel, K. John, C. Leterrier, S. L. Reck-Peterson, L. Blanchoin, M. Théry, Self-repair protects microtubules from destruction by molecular motors. *Nat. Mater.* **20**, 883–891 (2021).
18. W. Zheng, B. R. Brooks, S. Doniach, D. Thirumalai, Network of dynamically important residues in the open/closed transition in polymerases is strongly conserved. *Structure* **13**, 565–577 (2005).
19. R. Tehver, J. Chen, D. Thirumalai, Allostery wiring diagrams in the transitions that drive the GroEL reaction cycle. *J. Mol. Biol.* **387**, 390–406 (2009).
20. I. Bahar, A. Atilgan, B. Berman, Direct evaluation of thermal fluctuations in proteins using a single-parameter harmonic potential. *Fold. Des.* **2**, 173–181 (1997).
21. I. Bahar, A. J. Rader, Coarse-grained normal mode analysis in structural biology. *Curr. Opin. Struct. Biol.* **15**, 586–592 (2005).
22. A. R. Atilgan, S. R. Durell, R. L. Jernigan, M. C. Demirel, O. Keskin, I. Bahar, Anisotropy of fluctuation dynamics of proteins with an elastic network model. *Biophys. J.* **80**, 505–515 (2001).
23. A. Vilfan, E. Frey, F. Schwabl, M. Thormählen, Y. H. Song, E. Mandelkow, Dynamics and cooperativity of microtubule decoration by the motor protein kinesin. *J. Mol. Biol.* **312**, 1011–1026 (2001).
24. E. Muto, H. Sakai, K. Kaseda, Long-range cooperative binding of kinesin to a microtubule in the presence of ATP. *J. Cell Biol.* **168**, 691–696 (2005).
25. A. Yildiz, M. Tomishige, R. D. Vale, P. R. Selvin, Kinesin walks hand-over-hand. *Science* **303**, 676–678 (2004).
26. C. L. Asbury, A. N. Fehr, S. M. Block, Kinesin moves by an asymmetric hand-over-hand mechanism. *Science* **302**, 2130–2134 (2003).
27. V. R. Schief, J. Howard, Conformational changes during kinesin motility. *Curr. Opin. Cell Biol.* **13**, 19–28 (2001).
28. W. O. Hancock, J. Howard, Kinesin's processivity results from mechanical and chemical coordination between the ATP hydrolysis cycles of the two motor domains. *Proc. Natl. Acad. Sci. U.S.A.* **96**, 13147–13152 (1999).
29. T. Mori, R. D. Vale, M. Tomishige, How kinesin waits between steps. *Nature* **450**, 750–754 (2007).
30. S. Uchimura, Y. Oguchi, M. Katsuki, T. Usui, H. Osada, J.-i. Nikawa, S. Ishiwata, E. Muto, Identification of a strong binding site for kinesin on the microtubule using mutant analysis of tubulin. *EMBO J.* **25**, 5932–5941 (2006).
31. S. Uchimura, Y. Oguchi, Y. Hachikubo, S. Ishiwata, E. Muto, Key residues on microtubule responsible for activation of kinesin ATPase. *EMBO J.* **29**, 1167–1175 (2010).
32. I. Minoura, H. Takazaki, R. Ayukawa, C. Saruta, Y. Hachikubo, S. Uchimura, T. Hida, H. Kamiguchi, T. Shimogori, E. Muto, Reversal of axonal growth defects in an extraocular fibrosis model by engineering the kinesin–microtubule interface. *Nat. Commun.* **7**, 10058 (2016).
33. G. M. Alushin, G. C. Lander, E. H. Kellogg, R. Zhang, D. Baker, E. Nogales, High-resolution microtubule structures reveal the structural transitions in αβ-tubulin upon GTP hydrolysis. *Cell* **157**, 1117–1129 (2014).
34. R. Zhang, G. M. Alushin, A. Brown, E. Nogales, Mechanistic origin of microtubule dynamic instability and its modulation by EB proteins. *Cell* **162**, 849–859 (2015).
35. J. Löwe, H. Li, K. H. Downing, E. Nogales, Refined structure of αβ-tubulin at 3.5 Å resolution. *J. Mol. Biol.* **313**, 1045–1057 (2001).
36. R. A. Cross, Review: Mechanochemistry of the kinesin-1 ATPase. *Biopolymers* **105**, 476–482 (2016).
37. R. D. Vale, Switches, latches, and amplifiers: Common themes of g proteins and molecular motors. *J. Cell Biol.* **135**, 291–302 (1996).
38. M. Kikkawa, E. P. Sablin, Y. Okada, H. Yajima, R. J. Fletterick, N. Hirokawa, Switch-based mechanism of kinesin motors. *Nature* **411**, 439–445 (2001).
39. M. Kikkawa, N. Hirokawa, High-resolution cryo-EM maps show the nucleotide binding pocket of KIF1a in open and closed conformations. *EMBO J.* **25**, 4187–4194 (2006).
40. H. Onishi, N. Mochizuki, M. F. Morales, On the myosin catalysis of ATP hydrolysis. *Biochemistry* **43**, 3757–3763 (2004).
41. S. Rice, A. W. Lin, D. Safer, C. L. Hart, N. Naber, B. O. Carragher, S. M. Cain, E. Pechatnikova, E. M. Wilson-Kubalek, M. Whittaker, E. Pate, R. Cooke, E. W. Taylor, R. A. Milligan, R. D. Vale, A structural change in the kinesin motor protein that drives motility. *Nature* **402**, 778–784 (1999).
42. C. M. Farrell, A. T. Mackey, L. M. Klumpp, S. P. Gilbert, The role of ATP hydrolysis for kinesin processivity. *J. Biol. Chem.* **277**, 17079–17087 (2002).
43. L. M. Klumpp, A. T. Mackey, C. M. Farrell, J. M. Rosenberg, S. P. Gilbert, A kinesin switch I arginine to lysine mutation rescues microtubule function. *J. Biol. Chem.* **278**, 39059–39067 (2003).
44. M. Yun, X. Zhang, C.-G. Park, H.-W. Park, S. A. Endow, A structural pathway for activation of the kinesin motor ATPase. *EMBO J.* **20**, 2611–2618 (2001).
45. T. J. Minehardt, R. Cooke, E. Pate, P. A. Kollman, Molecular dynamics study of the energetic, mechanistic, and structural implications of a closed phosphate tube in ncd. *Biophys. J.* **80**, 1151–1168 (2001).
46. Y. Z. Ma, E. W. Taylor, Mechanism of microtubule kinesin ATPase. *Biochemistry* **34**, 13242–13251 (1995).
47. R. Nitta, Y. Okada, N. Hirokawa, Structural model for strain-dependent microtubule activation of Mg-ADP release from kinesin. *Nat. Struct. Mol. Biol.* **15**, 1067–1075 (2008).
48. N. Naber, S. Rice, M. Matuska, R. D. Vale, R. Cooke, E. Pate, EPR spectroscopy shows a microtubule-dependent conformational change in the kinesin switch 1 domain. *Biophys. J.* **84**, 3190–3196 (2003).
49. K. Sekimoto, J. Prost, Elastic anisotropy scenario for cooperative binding of kinesin-coated beads on microtubules. *J. Phys. Chem. B* **120**, 5953–5959 (2016).
50. R. Zhang, B. LaFrance, E. Nogales, Separating the effects of nucleotide and EB binding on microtubule structure. *Proc. Natl. Acad. Sci. U.S.A.* **115**, E6191–E6200 (2018).
51. H. Li, D. J. DeRosier, W. V. Nicholson, E. Nogales, K. H. Downing, Microtubule structure at 8 Å resolution. *Structure* **10**, 1317–1328 (2002).
52. J. Atherton, I. Farabella, I.-M. Yu, S. S. Rosenfeld, A. Houdusse, M. Topf, C. A. Moores, Conserved mechanisms of microtubule-stimulated ADP release, ATP binding, and force generation in transport kinesins. *eLife* **3**, e03680 (2014).

Acknowledgments: We thank N. Hori, M. L Mugnai, and R. A. Cross for discussions.
Funding: D.T. is grateful to NSF (CHE 19-000033) for support. Additional support from the Welch Foundation, through the Collie-Welch Chair (F-0019), is acknowledged. H.T.V. is currently funded through an EMBO Long-term Postdoctoral Fellowship (EMBO ALTF 904-2019). **Author contributions:** Conceptualization: H.T.V., Z.Z., R.T., and D.T. Methodology: H.T.V., Z.Z., R.T., and D.T. Investigation: H.T.V. and Z.Z. Visualization: H.T.V. and Z.Z. Supervision: D.T. Writing—original draft: H.T.V., Z.Z., R.T., and D.T. Writing—review and editing: H.T.V., R.T., and D.T. **Competing interests:** The authors declare that they have no competing interests. **Data and materials availability:** All data needed to evaluate the conclusions in the paper are present in the paper and/or the Supplementary Materials. The ENM code can be found here: https://doi.org/10.5281/zenodo.6113351. The raw data of all the graphs are also available at https://doi.org/10.5281/zenodo.6113088.

Submitted 2 November 2021
Accepted 24 February 2022
Published 13 April 2022
10.1126/sciadv.abn0856